

Spin-triplet p -wave pairing in a 3-orbital model for iron pnictide superconductors

Patrick A. Lee and Xiao-Gang Wen

Department of Physics, Massachusetts Institute of Technology, Cambridge, MA 02139, USA

(Dated: July 26, 2021)

We examine the possibility that the superconductivity in the newly discovered FeAs materials may be caused by the Coulomb interaction between d -electrons of the iron atoms. We find that when the Hund's rule ferromagnetic interaction is strong enough, the leading pairing instability is in spin-triplet p -wave channel in the weak coupling limit. The resulting superconducting gap has nodal points on the 2D Fermi surfaces. The \mathbf{k} dependent hybridization of several orbitals around a Fermi pocket is the key for the appearance of the spin-triplet p -wave pairing.

I. INTRODUCTION

Recently, a new class of superconductors – iron based superconductors – was discovered.^{1–10} The superconducting transition temperature can be as high as 52K.⁸ The undoped samples (for example LaOFeAs) appear to have a spin ordered phase below 150K.^{5,9,10} The electron doped² LaO_{1-x}F_xFeAs and hole doped⁴ LaO_{1-x}Sr_xFeAs samples are superconducting with $T_c \sim 25$ K. The magnetic field dependence of the specific heat in the electron doped material suggests the presence of gapless nodal lines on the Fermi surface.³

It appears that the electron-phonon interaction is not strong enough to give rise to such high transition temperature.¹¹ In this paper, we will examine the possibility that Coulomb interaction between d -electrons on Fe drives the superconductivity in the electron/hole doped samples and the spin-order in the undoped samples. In this case, we find that a p -wave spin-triplet superconducting order with gapless nodal lines is the most likely superconducting order in the weak coupling limit. Naively short range repulsion does not have the requisite \mathbf{k} dependence to drive p -wave pairing. It turns out that the \mathbf{k} dependent hybridization of several orbitals around a Fermi pocket makes the p -wave spin-triplet pairing possible. The same model is also shown to have spin-density wave (SDW) order for undoped samples.

II. A THREE-ORBITAL TIGHT-BINDING MODEL

First, let us examine the Fermi surfaces of the iron-based superconductor. For concreteness, we will consider the LaOFeAs sample. We will assume that the properties of the sample are mainly determined by the Fe-As planes. The Fe atoms in a Fe-As plane form a 2D square lattice (see Fig. 1). Due to the buckling of the As atoms, the real unit cell contains two Fe atoms. The real unit cell is also a square (see Fig. 1). According to band structure calculations, the Fermi surfaces of the Fe d -bands are formed by two hole pockets at the Γ point and two electron pocket at the M point (see Fig. 2a).^{12–15} All those pockets, mainly formed by the d_{xz} , d_{yz} and d_{xy} orbitals of Fe,¹¹ have similar size, shape, and Fermi velocity.

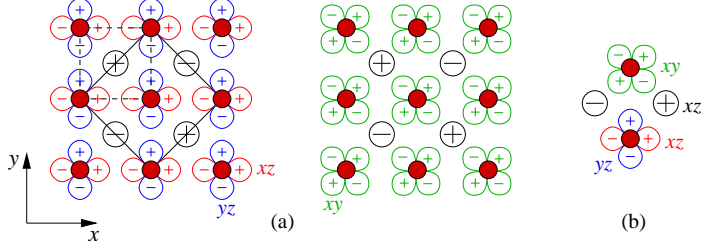


FIG. 1: (Color online) (a) The Fe-As plane and the d -orbitals of Fe. The filled dots are Fe atoms and the empty dots are As atoms. The plus and minus signs in the empty dots indicate if the As atom is above or below the Fe plane. The large square is the 2D unit cell. The dashed square is the reduced unit cell which contains only one Fe. The d_{xz} , d_{yz} and d_{xy} orbitals of the Fe atoms are described by the red, blue and green curves respectively. (b) The y hopping between the d_{xz} or d_{yz} with d_{xy} orbitals.

To understand the mixing of the orbitals near those Fermi pockets, we follow Ref. 13,14 to unfold the band structure to the extended Brillouin zone (BZ). Ordinarily, such an unfolding of the band structure extends the BZ superficially and there are certain ambiguities in assigning the location of each band. We emphasize that this is not the case here. The band structure of the extended BZ is uniquely defined due to an additional symmetry, *i.e.* the Fe-As plane is invariant under $P_z T_x$ and $P_z T_y$, where T_x (T_y) is the translation in the x (y) direction by the Fe-Fe distance and P_z is the reflection $z \rightarrow -z$ (see Fig. 1). Thus, if we combine the translation and the reflection P_z , then the electron hopping Hamiltonian H has a symmetry described by a reduced unit cell with only one Fe per unit cell (see Fig. 1). Since $[P_z T_x, H] = [P_z T_y, H] = [P_z T_x, P_z T_y] = 0$, we can use the eigenvalues of $P_z T_x$ and $P_z T_y$ to label the single-body energy eigenstates:

$$P_z T_x |\tilde{\mathbf{k}}\rangle = e^{i\tilde{k}_x} |\tilde{\mathbf{k}}\rangle, \quad P_z T_y |\tilde{\mathbf{k}}\rangle = e^{i\tilde{k}_y} |\tilde{\mathbf{k}}\rangle, \quad (1)$$

where $\tilde{\mathbf{k}} = (\tilde{k}_x, \tilde{k}_y)$ plays a role of crystal momentum. We will use such a pseudo crystal momentum to label states in an energy band. It is the pseudo crystal momenta $\tilde{\mathbf{k}}$ that form the extended Brillouin zone (see Fig. 2b) which corresponds to the reduced unit cell with only one Fe.

Let us work out an explicit example by considering a

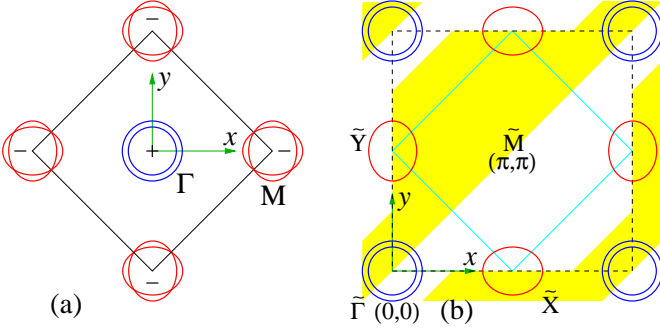


FIG. 2: (Color online) (a) The Fermi surfaces of the Fe d -bands. The plus sign marks the hole pockets and the minus sign marks the electron pockets. The square is the Brillouin zone. (b) The extended Brillouin zone (dashed square) for the reduce unit cell and the positions of the Fermi pockets in the extended Brillouin zone. The $\tilde{\Gamma}$ point has $(\tilde{k}_x, \tilde{k}_y) = (0, 0)$. The folding of the extended Brillouin zone in (b) produces (a). After folding, the $(\tilde{\Gamma}, \tilde{M})$ and (\tilde{X}, \tilde{Y}) in the extended Brillouin zone map into the Γ and M in the original Brillouin zone, respectively. The yellow shading marks the region where the p -wave pairing order parameter may have the same sign.

tight-binding model involving the d_{xz} , d_{yz} and d_{xy} orbitals. First, consider the hopping terms that do not mix the orbitals:

$$H_1 = - \sum_{\langle ij \rangle} [t_{ij}^{xz} (c_i^{xz})^\dagger c_j^{xz} + t_{ij}^{yz} (c_i^{yz})^\dagger c_j^{yz} + t_{ij}^{xy} (c_i^{xy})^\dagger c_j^{xy} + h.c.] \quad (2)$$

where i, j label the positions of the Fe. Since the d_{xz} , d_{yz} and d_{xy} orbitals are eigenstates of P_z reflection, the $P_z T_x$ and $P_z T_y$ symmetries require that t_{ij}^{xz} , t_{ij}^{yz} , and t_{ij}^{xy} only depend on $i - j$. The mixing term between the d_{xz} and d_{yz} orbitals is given by

$$H_2 = - \sum_{\langle ij \rangle} [t_{ij}^{xz,yz} (c_i^{xz})^\dagger c_j^{yz} + h.c.], \quad (3)$$

where $t_{ij}^{xz,yz}$ also depends only on $i - j$ as required by the $P_z T_x$ and $P_z T_y$ symmetries. On the other hand, the mixing term between the d_{xz} and d_{xy} orbitals as well as that between the d_{yz} and d_{xy} orbitals are given by

$$H_3 = \sum_{\langle ij \rangle} (-)^{i_x+i_y} [t_{ij}^{xz,xy} (c_i^{xz})^\dagger c_j^{xy} + t_{ij}^{yz,xy} (c_i^{yz})^\dagger c_j^{xy} + h.c.], \quad (4)$$

where $t_{ij}^{xz,xy}$, and $t_{ij}^{yz,xy}$ only depend on $i - j$. We note that the d_{xz} and d_{xy} orbitals have opposite eigenvalues ± 1 under P_z . The $P_z T_x$ and $P_z T_y$ symmetries require the presence of the factor $(-)^{i_x+i_y}$. Thus, c^{xz} and c^{yz} with conventional crystal momentum $\mathbf{k} + \mathbf{Q}$ can mix with $c_{\mathbf{k}}^{xy}$ with crystal momentum \mathbf{k} where $\mathbf{Q} = (\pi, \pi)$.

However, in the pseudo crystal momentum $\tilde{\mathbf{k}}$ space, only operators with the same pseudo crystal momentum

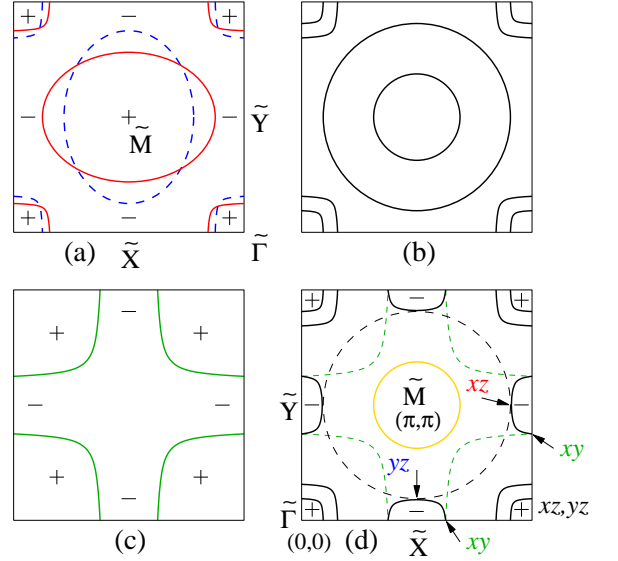


FIG. 3: (Color online) (a) The zero energy contour of $\epsilon_{xz}(\tilde{\mathbf{k}})$ (red) and $\epsilon_{yz}(\tilde{\mathbf{k}})$ (dashed blue). The \pm are signs of $\epsilon_{xz}(\tilde{\mathbf{k}})$ and $\epsilon_{yz}(\tilde{\mathbf{k}})$ in the region. The $\tilde{\Gamma}$ point has $\tilde{\mathbf{k}} = 0$ (b) The hybridization of the d_{xz} and d_{yz} bands. The curves are the zero energy contours of the hybridized bands. (c) The zero energy contour of $\epsilon_{xy}(\tilde{\mathbf{k}})$. (d) The solid curves are the Fermi surfaces of the three-band tight-binding model as a result of the hybridization of (b) and (c).

can mix. Let

$$\tilde{\Psi}_{\tilde{\mathbf{k}}} = (\tilde{c}_{\tilde{\mathbf{k}}}^{xz}, \tilde{c}_{\tilde{\mathbf{k}}}^{yz}, \tilde{c}_{\tilde{\mathbf{k}}}^{xy})^T \quad (5)$$

be the operators with pseudo crystal momentum $\tilde{\mathbf{k}}$, where

$$\begin{aligned} \tilde{c}_{\tilde{\mathbf{k}}}^{xz} &\sim \sum_i e^{-i(\tilde{\mathbf{k}}+\mathbf{Q})\cdot\mathbf{i}} c_i^{xz} \\ \tilde{c}_{\tilde{\mathbf{k}}}^{yz} &\sim \sum_i e^{-i(\tilde{\mathbf{k}}+\mathbf{Q})\cdot\mathbf{i}} c_i^{yz} \\ \tilde{c}_{\tilde{\mathbf{k}}}^{xy} &\sim \sum_i e^{-i\tilde{\mathbf{k}}\cdot\mathbf{i}} c_i^{xy} \end{aligned} \quad (6)$$

We see that the pseudo crystal momentum $\tilde{\mathbf{k}}$ and the conventional crystal momentum \mathbf{k} are related by $\mathbf{k} = \tilde{\mathbf{k}}$ for the d_{xy} orbital and $\mathbf{k} + \mathbf{Q} = \tilde{\mathbf{k}}$ for the d_{xz} and d_{yz} orbitals. The total hopping Hamiltonian $H = H_1 + H_2 + H_3$ can be written as $H = \sum_{\tilde{\mathbf{k}}} \tilde{\Psi}_{\tilde{\mathbf{k}}}^\dagger M_{\tilde{\mathbf{k}}} \tilde{\Psi}_{\tilde{\mathbf{k}}}$ with

$$M_{\tilde{\mathbf{k}}} = \begin{pmatrix} \epsilon_{xz}(\tilde{\mathbf{k}}) & \epsilon_{xz,yz}(\tilde{\mathbf{k}}) & \epsilon_{xz,xy}(\tilde{\mathbf{k}}) \\ \epsilon_{xz,yz}(\tilde{\mathbf{k}}) & \epsilon_{yz}(\tilde{\mathbf{k}}) & \epsilon_{yz,xy}(\tilde{\mathbf{k}}) \\ \epsilon_{xz,xy}^*(\tilde{\mathbf{k}}) & \epsilon_{yz,xy}^*(\tilde{\mathbf{k}}) & \epsilon_{xy}(\tilde{\mathbf{k}}) \end{pmatrix}. \quad (7)$$

It is worth noting that the above Hamiltonian and the resulting energy bands are defined on the extended Brillouin zone (labeled by $\tilde{\mathbf{k}}$) of the reduced unit cell (see Fig. 2b).

The nearest neighbor admixture between d_{xz} and d_{yz} vanishes by symmetry. Keeping the next nearest neighbor term only, we have $\epsilon_{xz,yz} = -2t'_{xz,yz} [\cos(\tilde{k}_x + \tilde{k}_y) -$

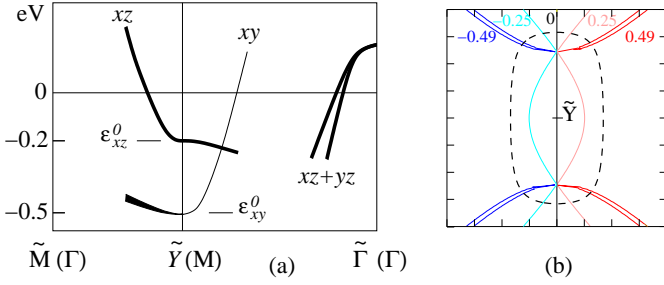


FIG. 4: (a) The energy bands near \tilde{Y} and $\tilde{\Gamma}$. The bands near \tilde{Y} come from the d_{xz} and d_{xy} orbitals. The thickness of the curve indicates the weight in the d_{xz} orbital. The bands near $\tilde{\Gamma}$ came from the d_{xz} and d_{yz} orbitals. (b) The contour plot of $i u_{\mathbf{k}} v_{\mathbf{k}}$ near \tilde{Y} . The dashed loop is the Fermi surface.

$\cos(\tilde{k}_x - \tilde{k}_y)$. Note that this vanishes at $\tilde{\Gamma}$, \tilde{M} , \tilde{X} and \tilde{Y} points (see Fig. 3), but is maximal midway between \tilde{X} and \tilde{Y} . Next, consider the nearest neighbor admixture between d_{xz} or d_{yz} with d_{xy} along the y direction (see Fig. 1b). These orbitals can admix only because of the asymmetry introduced by the As ions, which has xz symmetry. This implies that the d_{xz} - d_{xy} overlap integral is odd under $x \rightarrow -x$ and vanishes. Only the d_{yz} - d_{xy} matrix element survives. Also note that under the 180° rotation in the x - y plane about the \mathbf{i} site, $(c_{\mathbf{i}+\mathbf{y}}^{yz})^\dagger c_{\mathbf{i}}^{xy} \rightarrow -(c_{\mathbf{i}-\mathbf{y}}^{yz})^\dagger c_{\mathbf{i}}^{xy}$. Thus only the combination $(c_{\mathbf{i}+\mathbf{y}}^{yz})^\dagger c_{\mathbf{i}}^{xy} - (c_{\mathbf{i}-\mathbf{y}}^{yz})^\dagger c_{\mathbf{i}}^{xy}$ that preserves such a symmetry can appear in the hopping Hamiltonian which has a form

$$\begin{aligned} & \sum_{\mathbf{i}} \left[(-)^{i_x+i_y} t_{yz,xy} [(c_{\mathbf{i}+\mathbf{y}}^{yz})^\dagger c_{\mathbf{i}}^{xy} - (c_{\mathbf{i}-\mathbf{y}}^{yz})^\dagger c_{\mathbf{i}}^{xy}] + h.c. \right] \\ &= \sum_{\mathbf{k}} \left[-t_{yz,xy} (e^{i\tilde{k}_y} - e^{-i\tilde{k}_y}) (\tilde{c}_{\mathbf{k}}^{yz})^\dagger \tilde{c}_{\mathbf{k}}^{xy} + h.c. \right] \quad (8) \end{aligned}$$

This allows us to conclude that the nearest neighbor d_{xz} - d_{xy} and d_{yz} - d_{xy} mixing give rise to $\epsilon_{xz,xy}(\mathbf{k}) = -2it_{xz,xy} \sin(\tilde{k}_x)$ and $\epsilon_{yz,xy}(\mathbf{k}) = -2it_{yz,xy} \sin(\tilde{k}_y)$.

Now we can see how the 3-orbital model can reproduce the four-pocket Fermi surface. Let us begin by assuming that $\epsilon_{xz}(\mathbf{k})$ lies just below the Fermi energy (-0.2eV) at $\mathbf{k} = \tilde{Y}$ and disperses rapidly upward towards \tilde{M} , reaching 2.5eV . From $\tilde{\Gamma}$, it descends towards \tilde{X} where its energy is -1.4eV . The dispersion is relatively flat along \tilde{X} - $\tilde{\Gamma}$ - \tilde{Y} and a shallow local maximum appear at $\tilde{\Gamma}$. The Fermi surface correspond to this band is shown in Fig. 3a. The d_{yz} band is similar except rotated by 90° . The reason for the choice of locating the $d_{xz} + d_{xy}$ band at \tilde{Y} (as opposed to \tilde{X}) will be explained later.

Next, we turn on the hybridization between d_{xz} and d_{yz} . The hybridization is maximal at X (midway between \tilde{X} and \tilde{Y}) and creates two sheets which touches at $\tilde{\Gamma}$ and two Fermi surfaces. We also find two concentric small hole pockets at $\tilde{\Gamma}$ which become the well known hole pockets at Γ after folding.

The d_{xy} band $\epsilon_{xy}(\mathbf{k})$ is assumed to be at -0.5eV at

$\tilde{\mathbf{k}} = \tilde{X}$ and $\tilde{\mathbf{k}} = \tilde{Y}$, and disperses rapid upwards toward $\tilde{\Gamma}$ but rather flat towards \tilde{M} . The Fermi surface is sketched in Fig. 3c. Now we turn on $\epsilon_{xz,xy}$ and $\epsilon_{yz,xy}$. This gives the electron pockets centered at \tilde{X} and \tilde{Y} which become the two electron pockets at M after the folding. Note that because $\epsilon_{xz,yz} = 0$ at \tilde{X} and \tilde{Y} , the band at \tilde{Y} (or \tilde{X}) is purely $d_{xz} + d_{xy}$ (or $d_{yz} + d_{xy}$). Furthermore, near \tilde{Y} , $\epsilon_{xz,xy} \sim \sin \tilde{k}_x$. Thus along \tilde{Y} - $\tilde{\Gamma}$, the hybridization is zero and the d_{xz} and d_{xy} bands cross as shown in Fig. 4a. Along \tilde{Y} - \tilde{M} , the upper band is mostly d_{xz} while the d_{xz} amplitude in the lower band increase linearly with the distance from \tilde{Y} . These features are in agreement with band calculations.^{11,14} and are strong evidences that our assignment of the d_{xz} band is correct.

The final result is an ellipse shaped pocket, with the long axis of the ellipse pointing in the y direction at \tilde{Y} (towards the hole pockets at $\tilde{\Gamma}$). The Fermi surface crossing along the long direction is purely d_{xy} and the short direction is mainly d_{xz} (see Fig. 3d).

The pocket formed between the dashed lines in Fig. 3d are eliminated for sufficiently strong hybridization. However, within the 3-orbital model, it is impossible remove the Fermi surface surrounding \tilde{M} (the gold solid loop in Fig. 3d), because the hybridization elements are all zero at \tilde{M} . We need a 4th band which crosses and hybridize with the $d_{xz} + d_{yz}$ band to eliminate the unwanted Fermi surface. Apart from this, the 4th band plays no role as far as the remaining two electron and two hole pockets are concerned. It is in this sense that we maintain that the 3-orbital model gives an adequate description of the low energy Hamiltonian.

III. THE INTERACTION BETWEEN d -ELECTRONS

Next, let us consider the single ion interaction between the electrons on the Fe d -orbitals which is given by

$$\begin{aligned} H_I &= \frac{1}{2} \sum_{\alpha, \alpha'} \int d^2\mathbf{x} d^2\mathbf{x}' c_{\alpha}^{\dagger}(\mathbf{x}) c_{\alpha}(\mathbf{x}) V(\mathbf{x} - \mathbf{x}') c_{\alpha'}^{\dagger}(\mathbf{x}') c_{\alpha'}(\mathbf{x}') \\ &= \frac{1}{2} \sum_{a_1, a_2, a_3, a_4, \alpha, \alpha'} c_{\alpha a_1}^{\dagger} c_{\alpha' a_2}^{\dagger} c_{\alpha' a_3} c_{\alpha a_4} \times \\ & \quad \int d^2\mathbf{x} d^2\mathbf{x}' \phi_{a_1}(\mathbf{x}) \phi_{a_2}(\mathbf{x}') V(\mathbf{x} - \mathbf{x}') \phi_{a_3}(\mathbf{x}') \phi_{a_4}(\mathbf{x}) \end{aligned} \quad (9)$$

where $a_1, \dots, a_4 = xz, yz, xy$ label the orbitals, $\phi_a(\mathbf{x})$ is the wave function of the orbitals, and c_a is the electron operator for the a -orbital. Due to the symmetry of the orbitals, a_i must appear in pairs and the above can be rewritten as

$$\begin{aligned} H_I &= \frac{1}{2} U_1 \sum_a c_{\alpha a}^{\dagger} c_{\beta a}^{\dagger} c_{\beta a} c_{\alpha a} + \frac{1}{2} U_2 \sum_{a \neq b} c_{\alpha a}^{\dagger} c_{\beta b}^{\dagger} c_{\beta b} c_{\alpha a} \\ &+ \frac{1}{2} J \sum_{a \neq b} c_{\alpha a}^{\dagger} c_{\beta b}^{\dagger} c_{\beta a} c_{\alpha b} + \frac{1}{2} J \sum_{a \neq b} c_{\alpha a}^{\dagger} c_{\beta a}^{\dagger} c_{\beta b} c_{\alpha b} \quad (10) \end{aligned}$$

where $U_1 = U_{aa} = U_{bb}$, $U_2 = U_{ab} = U_1 - 2J$,¹⁶ and

$$\begin{aligned} U_{ab} &= \int d^2\mathbf{x} d^2\mathbf{x}' \phi_a(\mathbf{x})\phi_b(\mathbf{x}')V(\mathbf{x} - \mathbf{x}')\phi_b(\mathbf{x}')\phi_a(\mathbf{x}), \\ J &= \int d^2\mathbf{x} d^2\mathbf{x}' \phi_a(\mathbf{x})\phi_b(\mathbf{x}')V(\mathbf{x} - \mathbf{x}')\phi_a(\mathbf{x}')\phi_b(\mathbf{x}). \end{aligned} \quad (11)$$

Here the U_1 term represents the Coulomb interaction between electrons on same orbital. The U_2 term represents the interaction between electrons on different orbitals. The first J term is the exchange effect that favor parallel spins on the same Fe and is responsible for the Hund's rule. The second J term is pair hopping between different orbitals.

IV. PAIRING INSTABILITY

The above d -electron interaction may cause a pairing instability. One possible pairing instability is the spin-triplet pairing between \tilde{X} and \tilde{Y} electron pockets.¹⁷ In this paper, we will consider a different type of pairing – the spin-triplet p -wave pairing within the same Fermi pocket.

First, let us consider the p -wave pairing on the Fermi pocket near the \tilde{Y} point (see Fig. 3). Such a Fermi pocket is a mixture of the d_{xz} and d_{xy} orbitals. Let ψ_{xz} and ψ_{xy} be the electron operators in the continuum limit in the d_{xz} and d_{xy} orbitals near the \tilde{Y} point. The electron operator ψ near the pocket at the \tilde{Y} point (see Fig. 2a) is a mixture of ψ_{xz} and ψ_{xy} .

The Hamiltonian has the $P_z P_x$, $P_z P_y$, P_{xy} , $P_z T_x$, and $P_z T_y$ symmetries, where $P_x : x \rightarrow -x$ and $P_y : y \rightarrow -y$ are reflections about a Fe atom. These symmetry dictates certain form of the continuum Hamiltonian. Alternatively, we can expand the tight-binding picture near \tilde{Y} to obtain the following form which respect all the symmetry requirements

$$\begin{aligned} H_0 &= (t_1 k_x^2 + t_2 k_y^2 + \epsilon_{xz}^0)\psi_{xz}^\dagger \psi_{xz} \\ &+ (\tilde{t}_1 k_x^2 + \tilde{t}_2 k_y^2 + \epsilon_{xy}^0)\psi_{xy}^\dagger \psi_{xy} + t_3 k_x (i\psi_{xy}^\dagger \psi_{xz} + h.c.) \end{aligned} \quad (12)$$

Here \mathbf{k} is the pseudo crystal momentum measured from the \tilde{Y} point. From Fig. 4(a), we see that the d_{xz} band is flat along the y -axis, which implies $t_1 \gg t_2$. Similarly $\tilde{t}_2 \gg \tilde{t}_1$. In the following, we will ignore t_2 and \tilde{t}_1 .

The electrons have two bands with energies

$$E_{\pm}(\mathbf{k}) = \epsilon_0 \pm \sqrt{\epsilon_2^2 + \epsilon_3^2}, \quad (13)$$

where

$$\begin{aligned} \epsilon_0 &= \frac{1}{2}(t_1 k_x^2 + \tilde{t}_2 k_y^2 + \epsilon_{xz}^0 + \epsilon_{xy}^0), \\ \epsilon_3 &= \frac{1}{2}(t_1 k_x^2 - \tilde{t}_2 k_y^2 + \epsilon_{xz}^0 - \epsilon_{xy}^0), \\ \epsilon_2 &= t_3 k_x. \end{aligned} \quad (14)$$

ψ_{xz} and ψ_{xy} are related to the electron operator ψ in the upper band E_+ as

$$\psi_{xz}(\mathbf{k}) = u_{\mathbf{k}}\psi(\mathbf{k}), \quad \psi_{xy}(\mathbf{k}) = v_{\mathbf{k}}\psi(\mathbf{k}), \quad (15)$$

where

$$\begin{aligned} u_{\mathbf{k}} &= \frac{i\epsilon_2}{\sqrt{2\epsilon_2^2 + 2\epsilon_3^2 - 2\epsilon_3\sqrt{\epsilon_2^2 + \epsilon_3^2}}}, \\ v_{\mathbf{k}} &= \frac{\epsilon_3 - \sqrt{\epsilon_2^2 + \epsilon_3^2}}{\sqrt{2\epsilon_2^2 + 2\epsilon_3^2 - 2\epsilon_3\sqrt{\epsilon_2^2 + \epsilon_3^2}}}. \end{aligned} \quad (16)$$

To obtain the pairing interaction near the \tilde{Y} point in the spin-triplet channel we set $\alpha = \beta = \alpha' = \beta' = \uparrow$ in (10). We find that the first and the fourth terms in (10) vanish. The second and the third terms become

$$\sum_{\mathbf{k}_1, \mathbf{k}_2} V_{\tilde{Y}}(\mathbf{k}_2, \mathbf{k}_1)[\psi_{\uparrow}(\mathbf{k}_2)\psi_{\uparrow}(-\mathbf{k}_2)]^\dagger \psi_{\uparrow}(\mathbf{k}_1)\psi_{\uparrow}(-\mathbf{k}_1) \quad (17)$$

in the spin-triplet and $(\mathbf{k}, -\mathbf{k})$ pairing channel, where the effective pairing interaction of ψ is

$$V_{\tilde{Y}}(\mathbf{k}_2, \mathbf{k}_1) = -(J - U_2)u_{\mathbf{k}_2}^* v_{-\mathbf{k}_2}^* u_{\mathbf{k}_1} v_{-\mathbf{k}_1} \quad (18)$$

From the effective pairing interaction, we can obtain a dimensionless coupling constant¹⁸

$$\lambda = -\frac{\int \frac{d\sigma_{\mathbf{k}}}{(2\pi)^2 |v_{\mathbf{k}}|} \int \frac{d\sigma_{\mathbf{k}'}}{(2\pi)^2 |v_{\mathbf{k}'}} g^*(\mathbf{k})V(\mathbf{k}, \mathbf{k}')g(\mathbf{k}')}{\int \frac{d\sigma_{\mathbf{k}}}{(2\pi)^2 |v_{\mathbf{k}}|} |g(\mathbf{k})|^2} \quad (19)$$

where $\int d\sigma_{\mathbf{k}}$ is the integration over the \tilde{Y} Fermi surface and $v_{\mathbf{k}}$ is the Fermi velocity. The function $g(\mathbf{k})$ is a square harmonics which describes the shape of the superconducting gap, e.g. $g(\mathbf{k}) = 1$ corresponds to an s -wave and $g(\mathbf{k}) = \sin k_x$ or $\sin k_y$ a p -wave superconductor. The superconducting transition temperature T_c is given by $T_c = \Omega e^{-1/\lambda}$, where Ω is of order of the Fermi energy of the pocket: $\Omega \sim 0.2\text{eV}$.

From (18), we find that, when $J > U_2$, the pairing interaction $V_{\tilde{Y}}(\mathbf{k}_2, \mathbf{k}_1)$ induces a pairing $g(\mathbf{k})$ that have the same symmetry as $u_{\mathbf{k}}v_{\mathbf{k}}$. Because $u_{\mathbf{k}}v_{\mathbf{k}}$ is odd in k_x (see Fig. 4b), the induced pairing is in p -wave channel $g(\mathbf{k}) = \sin k_x$. Thus when $J > U_2$, the d -electron interaction will cause a spin-triplet p -wave pairing. Note that the location of the node depends on the choice of $\sin k_x$ versus $\sin k_y$, which in turn hinges on our assignment of the orbital to be xz -like near \tilde{Y} . Triplet pairing has been proposed earlier,¹⁹ and fully gapped states such as $p_x + ip_y$ were suggested. In contrast, after including the \mathbf{k} -dependent orbital-mixing, we find the on-site ferromagnetic interaction to favor a particular nodal p_x and p_y states in the \tilde{Y} and \tilde{X} valleys respectively.

As long as $\epsilon_F > \epsilon_{xz}^0$, we see from Fig. 4a that the Fermi surface changes its character from pure d_{xy} to mostly d_{xz} as a function of angles. $|u_{\mathbf{k}}|^2$ and $|v_{\mathbf{k}}|^2$ must cross at some angles where $|u_{\mathbf{k}}v_{\mathbf{k}}|$ takes its peak value $1/2$ (see

Fig. 4b). Thus the effect of $|u_{\mathbf{k}}v_{\mathbf{k}}|$ or λ is relatively insensitive to doping provided that $\epsilon_F > \epsilon_{xz}^0$. Since the density of states is also independent of doping in 2D, this explains why T_c is somewhat insensitive to doping and may extended to the hole doped side,⁴ except near zero doping. There the U_1 term will drive an SDW instability due to the nesting between the electron and the hole pockets.^{23,13}

We would like to mention that since $E(\mathbf{k}) = E(-\mathbf{k})$, our intra-pocket p -wave pairing appears even when the attraction $J - U_2$ is weak. When the attraction $J - U_2$ is strong enough to overcome the inter-pocket energy splitting ($\sim 0.05\text{eV}$), our model also has the instability in the spin-triplet inter-pocket pairing channel proposed in Ref. 17. Since the intra-pocket effective attraction is reduced by the matrix elements as shown in (18), the inter-pocket pairing may be stronger in large $J - U_2$ limit while the intra-pocket pairing is stronger in small $J - U_2$ limit.

Similarly, we can consider the spin-triplet pairing on the Fermi pocket near the $\tilde{\Gamma}$ point (see Fig. 2b). Such a Fermi pocket is a mixture of the d_{xz} and d_{yz} orbitals. The dispersion and the d_{xz} - d_{yz} mixing near $\tilde{\Gamma}$ can be determined from the symmetry consideration. The crucial difference is that the hybridization matrix element is now proportional to $k_x k_y$. After a similar calculation, we find that the spin-triplet pairing potential $V_{\tilde{\Gamma}}(\mathbf{k}_2, \mathbf{k}_1)$ satisfy $V_{\tilde{\Gamma}}(\mathbf{k}_2, \mathbf{k}_1) = V_{\tilde{\Gamma}}(\mathbf{k}_2, -\mathbf{k}_1) = V_{\tilde{\Gamma}}(-\mathbf{k}_2, \mathbf{k}_1)$. A p -wave pairing will result in a vanishing dimensionless coupling $\lambda = 0$. Thus the Coulomb interaction in the d -orbitals does not induce spin-triplet p -wave pairing on the two pockets near $\tilde{\Gamma}$ even when $J > U_2$. We see that the d_{xz} - d_{xy} (d_{yz} - d_{xy}) mixing at \tilde{Y} (\tilde{X}) in the 3-orbital model is crucial for the appearance of our p -wave instability. A 2-orbital model has the wrong Fermi surface topology in that one hole pocket is located at $\tilde{\Gamma}$ and \tilde{M} in Fig. 2(b), instead of both being at $\tilde{\Gamma}$.²² Although the 2-orbital model may allow certain superconducting states,^{20,21} it does not have the proper symmetry and the orbital mixing to generate the p -wave pairing proposed here.

V. CONCLUSION

In this paper, we examine the possibility that Coulomb interaction between the electrons in the Fe d -orbitals may induce a superconducting phase. We find that when the Hund's rule ferromagnetic interaction on Fe is strong enough, *ie* when $J > U_2$, the Coulomb interaction can induce pairing instability. In the weak coupling limit, the leading instability is found to be a spin-triplet p -wave pairing on the electron pockets at \tilde{M} (or at \tilde{X} and \tilde{Y} in the extended Brillouin zone). Although the Coulomb interaction can only directly induce pairing on the electron pockets at \tilde{M} , the proximity effect will lead to a p -wave pairing on the hole pockets at $\tilde{\Gamma}$. So the resulting superconducting state has node lines on the 3D Fermi surfaces.

The spin triplet pairing order parameter is a complex vector \mathbf{d} . The relative phases and relative orientations of the two order parameters $\mathbf{d}_{\tilde{X}}$ and $\mathbf{d}_{\tilde{Y}}$ on the two pockets \tilde{X} and \tilde{Y} can have interesting relations which cannot be determined from the linear response calculation adopted here. One possible distribution of the phases is given in Fig. 2b, where p -wave pairing gap is positive in the shaded regions and negative in unshaded regions.

At the atomic level, $U \approx 3$ to 4 eV and $J \approx 0.7$ eV, so $U_2 - J$ is positive. However, in a tight binding model involving only the Fe d -orbitals, the As orbitals have been projected out and the appropriate U and J are those corresponding to the Wannier orbitals which are much more extended than the atomic d orbitals. A recent estimate by Anisimov *et al.*²⁴ found the average U to be strongly renormalized down to 0.8 eV while J remains large at 0.5 eV. These are the more appropriate bare parameters in a 3-band model. Furthermore, in a crystal, the strong hopping leads to extended quasiparticles near the Fermi surface. The on-site U_2 and J will induce effective interaction U_2^* and J^* between those quasiparticles. The term induced by U_2 will remain short ranged. However, J may induce a long range couple because parallel spin configuration favors hopping, *ie* Hund's rule and hopping are compatible. Since the Fermi pockets are small, the effective interaction is given by $U_2^*(q) - J^*(q)$ with $q \sim k_F \ll 1/a$. A long range J -coupling enhances $J^*(q=0)$ and can potentially lead to a sign change and a net effective attraction.

Since the original submission of this paper the experimental situation has evolved rapidly. Here we attempt a brief summary of the relevant experimental data. The issue of whether gap nodes exist remains open to debate. Photoemission data on $\text{Ba}_{1-x}\text{K}_x\text{Fe}_2\text{As}_2$ indicate an almost isotropic gap on the hole pocket in this hole doped material.²⁵ It was recently found that the magnetic field dependence of the specific heat in this material is linear,²⁶ in contrast with the \sqrt{H} behavior taken as evidence for nodes in the electron doped material.³ At the same time, the nuclear spin relaxation rate $\frac{1}{T_1}$ fits the T^3 law over three decades in $\text{La}(\text{O}_{1-x}\text{Fe}_x)\text{FeAs}$.²⁷ Thus at the moment, existing data seem to point to gap nodes in electron doped materials and their absence in hole doped materials. We note that, because the size of the Fermi pockets are small, it is usually advantageous to hide the nodes in the k space between Fermi pockets. In order to produce a gap node on the Fermi surface of the small pocket, one needs an effective pairing potential which varies rapidly on the scale of the small pocket. Our theory is one of the few that will do this, and we rely on the rapid k dependence of the hybridization matrix element. The message that wavefunction and matrix elements may play an important role and must therefore be handled properly has validity beyond the special p -wave pairing scenario described here.

What about singlet vs. triplet pairing? The Knight shift is probably the best way to answer this question. In a triplet superconductor, the spin contribution to the

Knight shift drops below T_c to zero if the magnetic field is parallel to the \mathbf{d} vector, but remains unchanged if it is perpendicular. If the \mathbf{d} vector is free to rotate, it will turn perpendicular to \mathbf{H} and no change in Knight shift is predicted. This is apparently the case for Sr_2RuO_4 . On the other hand, if \mathbf{d} is locked to the lattice, we expect to see in a polycrystalline sample a drop of 2/3 of the value compared with singlet pairing. Without accurate knowledge of the orbital contribution to the Knight shift, this is hard to distinguish. Thus NMR on single crystals is needed to settle this question. As of this writing, the only single crystal data available is from Ning *et al.*²⁸ on $\text{BaFe}_{1.8}\text{Co}_{0.2}\text{As}_2$. The data does not support triplet pairing in that a drop in the Knight shift is seen for field directions both parallel and perpendicular to the

plane. On the other hand, a recent paper by Nakai *et al.*²⁹ on the FeP system $\text{La}_{0.87}\text{Ca}_{0.13}\text{FePO}$ shows that the magnetic behavior is quite different from the FeAs system. The Knight shift increases with decreasing temperature, indicative of ferromagnetic fluctuations above T_c and $\frac{1}{T_1T}$ shows a very unusual increase below T_c . The authors speculate that magnetic fluctuations associated with triplet pairing may be responsible for the increase. The experimental situation remains in flux and it may be possible that different pairing scenarios may be competing and win out in different materials.

This research is supported by DOE grant DE-FG02-03ER46076 (PAL) and by NSF Grant DMR-0706078 (XGW).

-
- ¹ Y. Kamihara, H. Hiramatsu, M. Hirano, R. Kawamura, H. Yanagi, T. Kamiya, and H. Hosono, *J. Am. Chem. Soc.* **128**, 10012 (2006).
- ² Y. Kamihara, T. Watanabe, M. Hirano, and H. Hosono, *J. Am. Chem. Soc.* **130**, 3296 (2008).
- ³ G. Mu, X. Zhu, L. Fang, L. Shan, C. Ren, and H.-H. Wen (2008), arXiv:0803.0928.
- ⁴ H.-H. Wen, G. Mu, L. Fang, H. Yang, and X. Zhu (2008), arXiv:0803.3021.
- ⁵ J. Dong, H. J. Zhang, G. Xu, Z. Li, G. Li, W. Z. Hu, D. Wu, G. F. Chen, X. Dai, J. L. Luo, et al. (2008), arXiv:0803.3426.
- ⁶ X. H. Chen, T. Wu, G. Wu, R. H. Liu, H. Chen, and D. F. Fang (2008), arXiv:0803.3603.
- ⁷ G. F. Chen, Z. Li, D. Wu, G. Li, W. Z. Hu, J. Dong, P. Zheng, J. L. Luo, and N. L. Wang (2008), arXiv:0803.3790.
- ⁸ Z.-A. Ren, J. Yang, W. Lu, W. Yi, G.-C. Che, X.-L. Dong, L.-L. Sun, and Z.-X. Zhao (2008), arXiv:0803.4283.
- ⁹ C. de la Cruz, Q. Huang, J. W. Lynn, J. Li, W. R. II, J. L. Zarestky, H. A. Mook, G. F. Chen, J. L. Luo, N. L. Wang, et al. (2008), arXiv:0804.0795.
- ¹⁰ M. A. McGuire, A. D. Christianson, A. S. Sefat, R. Jin, E. A. Payzant, B. C. Sales, M. D. Lumsden, and D. Mandrus (2008), arXiv:0804.0796.
- ¹¹ L. Boeri, O. V. Dolgov, and A. A. Golubov (2008), arXiv:0803.2703.
- ¹² D. Singh and M. Du (2008), arXiv:0803.0429.
- ¹³ I. Mazin, D. Singh, M. Johannes, and M. Du (2008), arXiv:0803.2740.
- ¹⁴ K. Kuroki, S. Onari, R. Arita, H. Usui, Y. Tanaka, H. Kontani, and H. Aoki (2008), arXiv:0803.3325.
- ¹⁵ K. Haule, J. H. Shim, and G. Kotliar (2008), arXiv:0803.1279.
- ¹⁶ C. Castellani, C. R. Natoli, and J. Ranninger, *Phys. Rev. B* **18**, 4945 (1978).
- ¹⁷ X. Dai, Z. Fang, Y. Zhou, and F.-C. Zhang (2008), arXiv:0803.3982.
- ¹⁸ D. J. Scalapino, E. Loh, and J. E. Hirsch, *Phys. Rev. B* **35**, 6694 (1987).
- ¹⁹ G. Xu, W. Ming, Y. Yao, X. Dai, S. Zhang, and Z. Fang, *et al.*, arXiv:0803.1282 (2008).
- ²⁰ Q. Han, Y. Chen, Z. D. Wang, arXiv:0803.4346 (2008)
- ²¹ Tao Li, arXiv:0804.0536 (2008).
- ²² S. Raghu, X.-L. Qi, C.-X. Liu, D. Scalapino, and S.-C. Zhang, *et al.*, arXiv:0804.1113 (2008).
- ²³ Fengjie Ma and Zhong-Yi Lu, arXiv:0803.3286 (2008).
- ²⁴ V. I. Anisimov, Dm. M. Korotin, S. V. Streltsov, A. V. Kozhevnikov, J. Kunes, A. O. Shorikov, and M. A. Korotin, arXiv:0807.0547.
- ²⁵ H. Ding, P. Richard, K. Nakayama, K. Sugawara, T. Arakane, Y. Sekiba, A. Takayama, S. Souma, T. Sato, T. Takahashi, Z. Wang, X. Dai, Z. Fang, G. F. Chen, J. L. Luo and N. L. Wang, *Europhysics Letters* **83**, 47001 (2008).
- ²⁶ Gang Mu, Huiqian Luo, Zhaosheng Wang, Lei Shan, Cong Ren, and Hai-Hu Wen, arXiv:0808.2941.
- ²⁷ Yusuke Nakai, Kenji Ishida, Yoichi Kamihara, Masahiro Hirano, and Hideo Hosono, *J. Phys. Soc. Jpn.* **77**, 073701 (2008).
- ²⁸ F.L. Ning, K. Ahilan, T. Imai, A. S. Sefat, R. Jin, M. A. McGuire, B. C. Sales, and D. Mandrus, *J. Phys. Soc. Jpn.*, to appear.
- ²⁹ Yusuke Nakai, Kenji Ishida, Yoichi Kamihara, Masahiro Hirano, and Hideo Hosono, *Phys. Rev. Lett.* **101**, 077006 (2008).